INTERNATIONAL JOURNAL FOR NUMERICAL METHODS IN ENGINEERING
Int. J. Numer. Meth. Engng 2015; **102**:728–747
Published online 17 February 2015 in Wiley Online Library (wileyonlinelibrary.com). DOI: 10.1002/nme.4851

Gradient correction for polygonal and polyhedral finite elements

Cameron Talischi[1], Anderson Pereira[2], Ivan F. M. Menezes[2] and Glaucio H. Paulino[1,3,*,†]

[1]*Department of Civil and Environmental Engineering, University of Illinois at Urbana-Champaign, Urbana, IL, 61801, USA*
[2]*Pontifical Catholic University of Rio de Janeiro (PUC-Rio), Rio de Janeiro, Brazil*
[3]*School of Civil and Environmental Engineering, Georgia Institute of Technology, 790 Atlantic Drive Atlanta, GA 30332, USA*

SUMMARY

Previous studies have shown that the commonly used quadrature schemes for polygonal and polyhedral finite elements lead to consistency errors that persist under mesh refinement and subsequently render the approximations non-convergent. In this work, we consider minimal perturbations to the gradient field at the element level in order to restore polynomial consistency and recover optimal convergence rates when the weak form integrals are evaluated using quadrature. For finite elements of arbitrary order, we state the accuracy requirements on the underlying volumetric and boundary quadrature rules and discuss the properties of the resulting corrected gradient operator. We compare the proposed approach with the pseudo-derivative method developed by Belytschko and co-workers and, for linear elliptic problems, with our previous remedy that involves splitting of polynomial and non-polynomial of elemental energy bilinear form. We present several numerical results for linear and nonlinear elliptic problems in two and three dimensions that not only confirm the recovery of optimal convergence rates but also suggest that the global error levels are close to those of approximations obtained from exact evaluation of the weak form integrals. Copyright © 2015 John Wiley & Sons, Ltd.

Received 31 July 2014; Revised 7 November 2014; Accepted 11 November 2014

KEY WORDS: polygonal and polyhedral finite elements; generalized barycentric coordinates; quadrature error; gradient correction; pseudo-derivatives

1. INTRODUCTION

This paper addresses the issue of numerical integration for polygonal and polyhedral finite elements (see [1–5] and references therein for examples of applications of such schemes). Because of the non-polynomial nature of underlying basis functions, the use of available quadrature rules for integration of weak form integrals leads to errors that upset the convergence of resulting approximations. As discussed in [6], these errors stem from a lack of polynomial consistency of the discrete system and persist under mesh refinement. We have observed in this previous study that the patch test errors for a Poisson boundary value problem do not vanish with finer meshes. While it is possible to use higher-order quadrature rules to reduce this consistency error to acceptable levels, such a strategy is not computationally viable considering the high cost of computing basis functions and their gradients and the large number of quadrature points needed. The burden of numerical integration is more pronounced in three dimensions and for nonlinear boundary value problems.

For linear elliptic problems, a remedy is proposed in [6] (see also [7]) that is based on a decomposition of the energy bilinear form at the element level. This decomposition is at the heart of the

*Correspondence to: Glaucio H. Paulino, School of Civil and Environmental Engineering, Georgia Institute of Technology, 790 Atlantic Drive Atlanta, GA 30332, USA.
†E-mail: paulino@gatech.edu

so-called virtual element method [8–10] and is enabled by the use of local projection maps that split up the trial and test fields into their polynomial and non-polynomial components. Provided that the energy of the polynomial components are captured exactly, the patch test is satisfied and, more generally, the consistency errors are guaranteed to vanish at an optimal rate with mesh refinements. In the approach put forth in [6], quadrature is used to evaluate only the non-polynomial term in the energy expression thus ensuring polynomial consistency of the resulting discrete system.

Here, we propose an alternative scheme that can be used for discretization of both linear and non-linear boundary value problems. The key idea is to define a *discrete* or *corrected gradient map* that restores consistency when evaluating the weak form with quadrature. The corrected gradient field is constructed at the element level through a minimal perturbation to the exact gradient such that a discrete version of the divergence theorem featuring polynomial trial fields of suitable order and attendant volumetric and surface quadrature rules is satisfied. In this respect, the proposed scheme is similar to the so-called pseudo-derivative method of Krongauz and Belytschko [11], which was explored in [12] and [13] in the context of polygonal and polyhedral finite elements. While the pseudo-derivative is only defined at the quadrature points, the corrected gradient is a well-defined field over the domain with distinguishing properties that can be used in the analysis of the resulting discretization. For example, as we shall see, the perturbation defining the corrected gradient is itself a polynomial field that captures the error in the satisfaction of the discrete divergence theorem. Moreover, the corrected gradient operator coincides with the exact gradient when applied to polynomial fields or when the quadrature rule is compatible with the underlying finite element spaces (for example, no correction is made for classical iso-parametric quadrilateral and hexahedral finite elements with the usual Gauss quadrature). Finally, we note that the proposed approach can potentially be cast in the framework of the so-called gradient schemes (cf. [14]) that are described by independent but compatible reconstructions of a field and its gradient from the same set of degrees of freedom.

The remainder of this paper is organized as follows: In Section 2, we review generalized barycentric coordinates and present the construction of first-order and second-order H^1-conforming polygonal and polyhedral finite element spaces. The accuracy requirements on volumetric and surface quadrature rules along with particular examples of such rules are discussed in Section 4. The definition of corrected gradient and its properties are presented in Section 4, followed by the discussion of its use for a general elliptic problem in Section 5. In Section 6, we compare the proposed approach with the pseudo-gradient method and the scheme proposed in [6] for linear problems. Finally, several numerical studies are presented in Section 7 followed by concluding remarks in Section 8.

2. FINITE ELEMENT SPACES AND THEIR PROPERTIES

Let us begin with the two-dimensional setting and consider an n-gon E whose vertices, ordered counterclockwise, are located at $\boldsymbol{x}_1, \ldots, \boldsymbol{x}_n$. The set of functions $\varphi_1, \ldots, \varphi_n$ are called *generalized barycentric coordinates* for E if they are non-negative in the interior of E and can interpolate the linear fields exactly. The latter means that for all $p \in \mathcal{P}_1(E)$ [‡],

$$p(\boldsymbol{x}) = \sum_{i=1}^{n} p(\boldsymbol{x}_i)\varphi_i(\boldsymbol{x}), \qquad \forall \boldsymbol{x} \in E \tag{1}$$

As shown in [15], any set of functions satisfying these properties also satisfy the so-called Kronecker-delta property (that is, $\varphi_i(\boldsymbol{x}_j) = \delta_{ij}$), and have linear variation along the boundary of E. Consequently, if $\boldsymbol{x}$ lies on the edge connecting vertices $\boldsymbol{x}_i$ and $\boldsymbol{x}_{i+1}$, we have[§]

$$\varphi_i(\boldsymbol{x}) = 1 - \frac{|\boldsymbol{x} - \boldsymbol{x}_i|}{|\boldsymbol{x}_{i+1} - \boldsymbol{x}_i|}, \quad \varphi_{i+1}(\boldsymbol{x}) = \frac{|\boldsymbol{x} - \boldsymbol{x}_i|}{|\boldsymbol{x}_{i+1} - \boldsymbol{x}_i|}, \quad \varphi_j(\boldsymbol{x}) = 0,\ j \neq i, i+1 \tag{2}$$

[‡]Throughout the paper, $\mathcal{P}_k(E)$ denotes the set of kth-order polynomial functions over the domain E.
[§]We are using the convention that $\boldsymbol{x}_{n+1} = \boldsymbol{x}_1$ and $\boldsymbol{x}_0 = \boldsymbol{x}_n$.

DOI: 10.1002/nme

We use generalized barycentric coordinates as the basis for a first-order finite element space, denoted by $\mathcal{V}_1(E)$, with degrees of freedom associated with the vertices of E. Note that (1) implies $\mathcal{V}_1(E) \supseteq \mathcal{P}_1(E)$. Moreover, thanks to (2), $\mathcal{V}_1(E)$ can be used to construct H^1-conforming finite element spaces over polygonal meshes.

A second-order space on E can be constructed using pairwise products of barycentric coordinates. Following the work of [16], we define quadratic serendipity-type interpolants $\psi_1, \ldots, \psi_{2n}$ on E as follows

$$\psi_i(\boldsymbol{x}) = \sum_{j=1}^{n} \sum_{k=1}^{n} c_{jk}^{i} \varphi_j(\boldsymbol{x}) \varphi_k(\boldsymbol{x}) \tag{3}$$

The coefficients c_{jk}^{i} are prescribed such that ψ_i's satisfy the Kronecker-delta property and can interpolate quadratic functions exactly. Denoting by $\hat{\boldsymbol{x}}_i$ the midpoint of edge connecting $\boldsymbol{x}_i$ and $\boldsymbol{x}_{i+1}$, the coefficients are thus chosen so that

$$p(\boldsymbol{x}) = \sum_{i=1}^{n} \left[p(\boldsymbol{x}_i) \psi_i(\boldsymbol{x}) + p(\hat{\boldsymbol{x}}_i) \psi_{i+n}(\boldsymbol{x}) \right], \qquad \forall p \in \mathcal{P}_2(E) \tag{4}$$

and

$$\psi_i(\boldsymbol{x}_j) = \psi_{i+n}(\hat{\boldsymbol{x}}_j) = \delta_{ij}, \quad \psi_i(\hat{\boldsymbol{x}}_j) = \psi_{i+n}(\boldsymbol{x}_j) = 0, \qquad \forall i, j = 1, \ldots, n \tag{5}$$

Observe that ψ_{i+n} is the interpolant associated with the midpoint $\hat{\boldsymbol{x}}_i$. Moreover, the variation of each ψ_i on the boundary of the element is continuous and piecewise quadratic. A method for computing the coefficients c_{jk}^{i}, which depend on the geometry of E, can be found in [16].

The second-order finite element space, denoted by $\mathcal{V}_2(E)$, is given by the span of $\psi_1, \ldots, \psi_{2n}$ and will be used to define an H^1-conforming space on a polygonal mesh with degrees of freedom associated with the vertices and midpoints of the edges of the mesh. Observe that (4) implies $\mathcal{V}_2(E) \supseteq \mathcal{P}_2(E)$.

A number of generalized barycentric coordinates are available in the literature with different requirements on the geometry of E (see, for example, [15]). For the sake of concreteness, we will consider Wachspress coordinates [17] here though we emphasize that the main results of this paper apply to finite element schemes derived from other interpolation functions. Wachspress functions are valid for polygons that are strictly convex and can be written as [18]

$$\varphi_i(\boldsymbol{x}) = \frac{w_i(\boldsymbol{x})}{\sum_{j=1} w_j(\boldsymbol{x})} \tag{6}$$

where the weight functions $w_1, \ldots, w_n$ are given by

$$w_i(\boldsymbol{x}) = \frac{|\boldsymbol{n}_{i-1} \times \boldsymbol{n}_i|}{[(\boldsymbol{x}_i - \boldsymbol{x}) \cdot \boldsymbol{n}_{i-1}] \, [(\boldsymbol{x}_i - \boldsymbol{x}) \cdot \boldsymbol{n}_i]} \tag{7}$$

In this expression, $\boldsymbol{n}_i$ denotes the unit normal vector to edge connecting vertices $\boldsymbol{x}_i$ and $\boldsymbol{x}_{i+1}$. We refer to [19] for the study of behavior of Wachspress functions and, in particular, bounds on their gradients in terms of the geometric attributes of E. The numerical studies presented in Section 7 use element spaces $\mathcal{V}_k(E)$, with $k = 1$ and $k = 2$, defined using Wachspress coordinates.

We proceed to discuss finite element spaces on polyhedra in $\mathbb{R}^3$. Let E be a polyhedron whose boundary consists of planar polygonal faces, and suppose it has n vertices located at $\boldsymbol{x}_1, \ldots, \boldsymbol{x}_n$. We shall denote by $\mathcal{F}$ the set of faces forming the boundary of E, by $\mathcal{F}_i$ those faces that include $\boldsymbol{x}_i$, and by $\mathcal{F}_i^c = \mathcal{F} \backslash \mathcal{F}_i$ the remaining faces.

As in the two-dimensional case, one can define generalized barycentric coordinates $\varphi_1, \ldots, \varphi_n$ on E such that they satisfy the Kronecker-delta property and interpolate linear fields exactly. Additionally, each φ_i has linear variation along the edges of E and vanishes on $\mathcal{F}_i^c$, that is, the faces not incident on the associated vertex $\boldsymbol{x}_i$. Furthermore, the behavior of φ_i on each face in $\mathcal{F}_i$ is determined uniquely by the geometry of that face and independent of the shape of the element. These

DOI: 10.1002/nme

important properties together guarantee inter-element continuity, and subsequently H^1-conformity of finite element space defined on a polyhedral mesh using vertex degrees of freedom.

For the numerical studies presented in this paper, we have utilized Wachspress coordinates, as defined in [18] and analyzed in [19]. These coordinates are valid for elements that are not only convex but also simple. This means that, the collection $\mathcal{F}_i$ for each $i = 1, \ldots, n$ consists of exactly three faces. For such a polyhedron, Wachspress coordinate φ_i is again defined by (6) with weight functions

$$w_i(\boldsymbol{x}) = \frac{\left(\boldsymbol{n}_{F_i^1} \times \boldsymbol{n}_{F_i^2}\right) \cdot \boldsymbol{n}_{F_i^3}}{\left[(\boldsymbol{x}_i - \boldsymbol{x}) \cdot \boldsymbol{n}_{F_i^1}\right]\left[(\boldsymbol{x}_i - \boldsymbol{x}) \cdot \boldsymbol{n}_{F_i^2}\right]\left[(\boldsymbol{x}_i - \boldsymbol{x}) \cdot \boldsymbol{n}_{F_i^3}\right]} \tag{8}$$

In the previous expression, $\boldsymbol{n}_F$ denotes the outward unit normal vector to face F, and F_i^1, F_i^2, and F_i^3 are the faces in $\mathcal{F}_i$.

As before, we set $\mathcal{V}_1(E) = \operatorname{span}\{\varphi_1, \ldots, \varphi_n\}$ that by linear precision of the Wachspress coordinates includes $\mathcal{P}_1(E)$. While the construction of serendipity polyhedra, following the two-dimensional procedure of Rand *et al.* [16], is possible, we have elected to defer their study to a future work. We note, however, that the gradient correction approach described in Section 4 is applicable to quadratic polyhedra as well, though certain aspects of its implementation as well as the numerical studies of its performance require a separate examination.

3. QUADRATURE RULES AND ACCURACY REQUIREMENTS

On general polygonal and polyhedral elements, barycentric coordinates are usually non-polynomial functions. This is evident in the case of Wachspress functions from (6). As discussed in [6], the evaluation of weak form integrals involving barycentric coordinates and their gradients by means of available quadrature schemes will lead to errors that are persistent under mesh refinement. These errors motivate the development of gradient correction approach proposed in this work. In order to control the quadrature errors and restore polynomial consistency, the proposed correction approach requires the utilized quadrature schemes to respect certain minimal accuracy conditions, expressed in terms of their polynomial precision. In this section, we will state these requirements for volumetric and surface quadrature rules on a general element E and proceed to give particular instances of schemes that satisfy them. These specific rules are commonly used in the literature on polygonal and polyhedral discretization. The numerical studies in Section 7 employ these quadrature schemes.

Given a polyhedral (polygonal) finite element E, we will denote by $\fint_E$ the evaluation of the volume (area) integral $\int_E$ using quadrature. Similarly, we will use $\oint_{\partial E}$ to denote the numerical evaluation of surface (line) integral $\int_{\partial E}$. Throughout, we shall assume that the order k of the finite element space $\mathcal{V}_k(E)$ is fixed.

In the proposed correction scheme, the volumetric quadrature $\fint_E$ is assumed to be exact when the integrand is a polynomial field of order $2k - 2$. This means that the quadrature can integrate constant fields exactly when $k = 1$ and quadratic fields when $k = 2$. This requirement is motivated by the fact that we need integrals of the form

$$\int_E \boldsymbol{p} \cdot \nabla q \, \mathrm{d}\boldsymbol{x}, \qquad \int_E q \operatorname{div} \boldsymbol{p} \, \mathrm{d}\boldsymbol{x} \tag{9}$$

to be computed exactly when $\boldsymbol{p} \in [\mathcal{P}_{k-1}(E)]^d$ and $q \in \mathcal{P}_k(E)$. We will encounter integrals of this form in the next section (see, for example, Equation (23)).

There is an additional implicit assumption on the volume quadrature rule that it is sufficiently rich so as to eliminate the appearance of spurious elemental zero energy modes that can upset the stability of resulting discretization scheme. For instance, for $k = 1$, a one-point rule consisting of an integration point at the centroid of E with the volume $|E|$ as the weight respects the above precision requirement, but it may lead to spurious zero energy modes.

DOI: 10.1002/nme

The boundary quadrature $\oint_{\partial E}$ is required to integrate polynomial fields of order $2k-1$ on each face (edge in two-dimensions) of the element. The quadrature is therefore exact on piecewise linear and cubic fields for $k=1$ and $k=2$, respectively. With this requirement, we ensure that integrals of the form

$$\int_{\partial E} q\,(\boldsymbol{p}\cdot\boldsymbol{n})\,\mathrm{d}\boldsymbol{s} \tag{10}$$

are exact if $\boldsymbol{p}\in[\mathcal{P}_{k-1}(E)]^d$ and q is piecewise kth order polynomials on ∂E with $\boldsymbol{n}$ the unit normal vector to the boundary. Again, such integrals will appear in the next section when establishing properties of the corrected gradient (e.g., Equation (23)). For two-dimensional elements, functions in $\mathcal{V}_k(E)$ have kth order polynomial variation on ∂E, and so we have

$$\oint_{\partial E} v\,(\boldsymbol{p}\cdot\boldsymbol{n})\,\mathrm{d}s=\int_{\partial E} v(\boldsymbol{p}\cdot\boldsymbol{n})\mathrm{d}s,\qquad \forall v\in\mathcal{V}_k(E),\,\boldsymbol{p}\in[\mathcal{P}_{k-1}(E)]^2 \tag{11}$$

We next describe the quadrature schemes used for the numerical studies in this paper. The quadrature scheme $\fint_E$ over a polygon is defined by subdividing the element into triangles (by connecting an interior point to its vertices) and using available polynomially precise quadrature rules on each triangle. For $k=1$ and $k=2$, Dunavant rules with one and three integration points are used here. The computation of boundary integrals are carried out using the Gauss–Lobatto rules with one and three integration points for $k=1$ and $k=2$. For $k=2$, the integration points at the vertices and midpoint of the edges simplifies the evaluation of (10) because the degrees of freedom for the serendipity element correspond to point-wise evaluation at these points.

For volumetric integration in three dimensions, one possibility is to split the element into tetrahedra and use the available quadrature schemes on these subdomains. A more economical alternative for linear polyhedra that satisfies the polynomial precision requirement is proposed in [20]. The element is divided into tributary regions, each associated with a vertex, and the centroids and volumes of these regions are taken as the quadrature locations and weights. The region associated with a vertex is composed of pyramids formed by the centroid of the element, the midpoint of the edges incident on the vertex, and centroids of the incident faces (Figure 1). This scheme can integrate constant and linear fields exactly.

As for the boundary quadrature, the integration on each face is carried out by means of vertex quadrature rule that requires only the evaluation of the integrand at the vertices of the face. The face is split up into quadrilateral regions associated with its vertices by connecting the centroid to the midpoint of the edges of the faces. The quadrature weights are the areas of these quadrilateral regions. It can be shown that this scheme is exact for integration of linear fields (see Appendix of [7]).

4. CORRECTED GRADIENT AND ITS PROPERTIES

Given an element E, the correction of the gradient of functions in the local space $\mathcal{V}_k(E)$ is obtained from minimal perturbations that result in satisfaction of a discrete divergence theorem. More specifically, the *corrected* gradient of $v\in\mathcal{V}_k(E)$, henceforth denoted by $\nabla_{E,k}v$, is taken to be the vector field over E that solves the optimization problem

$$\min_{\boldsymbol{\xi}} \fint_E |\nabla v-\boldsymbol{\xi}|^2\,\mathrm{d}\boldsymbol{x} \tag{12}$$

subject to

$$\fint_E \boldsymbol{p}\cdot\boldsymbol{\xi}\,\mathrm{d}\boldsymbol{x}=-\fint_E v\,\mathrm{div}\,\boldsymbol{p}\mathrm{d}\boldsymbol{x}+\oint_{\partial E} v\,(\boldsymbol{p}\cdot\boldsymbol{n})\,\mathrm{d}\boldsymbol{s},\ \forall\,\boldsymbol{p}\in[\mathcal{P}_{k-1}(E)]^d \tag{13}$$

DOI: 10.1002/nme

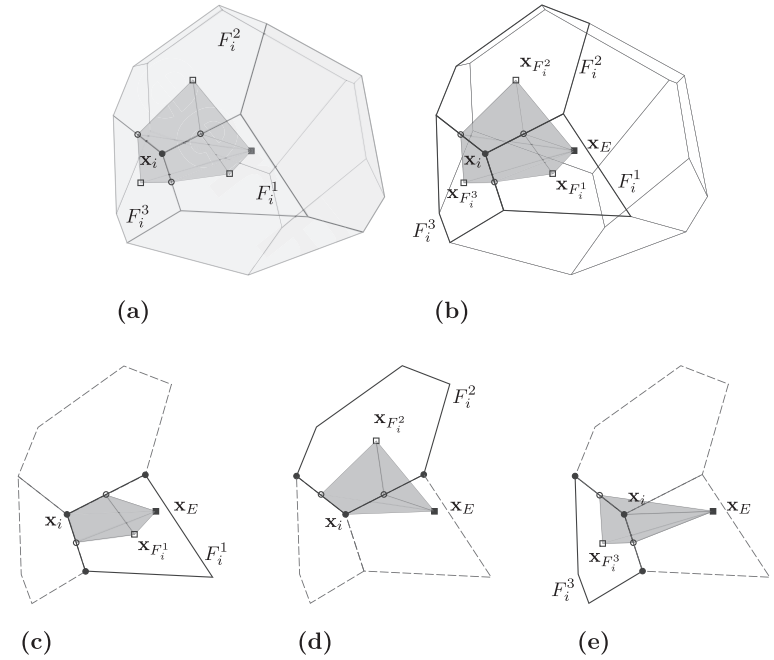

Figure 1. Illustration of volumetric quadrature rule for linear polyhedra. (a) Tributary region associated with vertex $\mathbf{x}_i$; the centroid of this region is a quadrature point; (b) the corresponding quadrature weight is the volume of the dark gray polyhedron formed by pyramids associated with faces incident on $\mathbf{x}_i$; and (c)–(e) the pyramid associated with a face F_i^j is formed by the centroid of the element $\mathbf{x}_E$, centroid of the face $\mathbf{x}_{F_i^j}$, and the midpoint of the edges of F_i^j incident on $\mathbf{x}_i$.

The minimization is carried out over all sufficiently smooth vector fields on E such that the quadrature makes sense. The corrected gradient $\nabla_{E,k} v$ is thus the 'closest'[¶] field to ∇v that satisfies the discrete divergence theorem against all polynomials of order k.

To better understand the nature of the gradient correction, let us consider a basis $\{\boldsymbol{p}_1, \ldots, \boldsymbol{p}_n\}$ for $[\mathcal{P}_{k-1}(E)]^d$ and replace (13) by the equivalent set of constraints:

$$\fint_E \boldsymbol{p}_\alpha \cdot \boldsymbol{\xi} \, \mathrm{d}\boldsymbol{x} = -\fint_E v \operatorname{div} \boldsymbol{p}_\alpha \mathrm{d}\boldsymbol{x} + \oint_{\partial E} v \, (\boldsymbol{p}_\alpha \cdot \boldsymbol{n}) \, \mathrm{d}\boldsymbol{s}, \ \alpha = 1, \ldots, n \tag{14}$$

Introducing multipliers $\lambda_1, \ldots, \lambda_n$, the Lagrangian for this optimization problem is given by

$$\begin{aligned} \mathcal{L}(\boldsymbol{\xi}, \lambda_1, \ldots, \lambda_n) = & \fint_E |\boldsymbol{\xi} - \nabla v|^2 \, \mathrm{d}\boldsymbol{x} \\ & + \sum_{\alpha=1}^{n} \lambda_\alpha \left[\fint_E \boldsymbol{p}_\alpha \cdot \boldsymbol{\xi} \, \mathrm{d}\boldsymbol{x} + \fint_E v \operatorname{div} \boldsymbol{p}_\alpha \mathrm{d}\boldsymbol{x} - \oint_{\partial E} v \, (\boldsymbol{p}_\alpha \cdot \boldsymbol{n}) \, \mathrm{d}\boldsymbol{s} \right] \end{aligned} \tag{15}$$

The optimality of $\nabla_{E,k} v$ requires that for any variation $\boldsymbol{\eta}$

$$D_{\boldsymbol{\xi}} \mathcal{L}(\nabla_{E,k} v, \lambda_1, \ldots, \lambda_n)[\boldsymbol{\eta}] = 2 \fint_E \left(\nabla_{E,k} v - \nabla v \right) \cdot \boldsymbol{\eta} \mathrm{d}\boldsymbol{x} + \sum_{\alpha=1}^{n} \lambda_\alpha \fint_E \boldsymbol{p}_\alpha \cdot \boldsymbol{\eta} \mathrm{d}\boldsymbol{x} = 0$$

[¶]The distance here is with respect to the quadrature form of the L^2-metric.

DOI: 10.1002/nme

and therefore

$$\fint_E \left(\nabla_{E,k} v - \nabla v + \sum_{\alpha=1}^{n} \frac{1}{2} \lambda_\alpha \boldsymbol{p}_\alpha \right) \cdot \boldsymbol{\eta} \mathrm{d}\boldsymbol{x} = 0 \tag{16}$$

This shows that the perturbation $\nabla_{E,k} v - \nabla v$ coincides with an element of $[\mathcal{P}_{k-1}(E)]^d$ at the location of the quadrature points. Observe that the optimization problem (12) and (13) can only prescribe the values of $\nabla_{E,k} v$ at the quadrature points. This motivates us to *define* the corrected gradient $\nabla_{E,k} v$ as the field satisfying the following two conditions:

C1: $\nabla_{E,k} v - \nabla v \in [\mathcal{P}_{k-1}(E)]^d$
C2: For all $\boldsymbol{p} \in [\mathcal{P}_{k-1}(E)]^d$,

$$\fint_E \boldsymbol{p} \cdot \nabla_{E,k} v \mathrm{d}\boldsymbol{x} = -\fint_E v \operatorname{div} \boldsymbol{p} \mathrm{d}\boldsymbol{x} + \oint_{\partial E} v \, (\boldsymbol{p} \cdot \boldsymbol{n}) \, \mathrm{d}\boldsymbol{s} \tag{17}$$

Note from these two conditions that $\nabla_{E,k}$ is a linear map and so in practice only the action of $\nabla_{E,k}$ on the basis of $\mathcal{V}_k(E)$ must be computed. The appendix contains details on a systematic procedure for computing the corrected gradient of the basis functions for an arbitrary k.

To better understand the nature of the correction, let us denote by $\boldsymbol{p}_v$ the perturbation to ∇v that gives the corrected gradients, that is,

$$\nabla_{E,k} v = \nabla v + \boldsymbol{p}_v \tag{18}$$

Inserting in C2, we get for $\boldsymbol{p} \in [\mathcal{P}_{k-1}(E)]^d$

$$\fint_E \boldsymbol{p} \cdot \boldsymbol{p}_v \mathrm{d}\boldsymbol{x} = \left[-\fint_E v \operatorname{div} \boldsymbol{p} \mathrm{d}\boldsymbol{x} + \oint_{\partial E} v \, (\boldsymbol{p} \cdot \boldsymbol{n}) \, \mathrm{d}\boldsymbol{s} \right] - \fint_E \boldsymbol{p} \cdot \nabla v \mathrm{d}\boldsymbol{x} \tag{19}$$

First, observe that the left-hand side integral is computed exactly by the quadrature. On the right-hand side of the previous expression, the term in the bracket and the last term represent two different quadrature approximations of $\int_E \boldsymbol{p} \cdot \nabla v \mathrm{d}\boldsymbol{x}$. Thus, (19) shows that the perturbations $\boldsymbol{p}_v$ captures the difference between two approximations of ∇v when integrated against polynomials of order $k-1$. Returning to the optimization problem (12) and (13), $\boldsymbol{p}_v$ is in fact the 'smallest' element in $[\mathcal{P}_{k-1}(E)]^d$, with respect to the L^2-norm, that does so. Moreover, the smaller the error in the satisfaction of the discrete divergence theorem (i.e., right-hand side of (19)), the smaller the perturbation to the gradient. This error depends on the accuracy of quadrature as well as the nature of the functions in the local space $\mathcal{V}_k(E)$.

These observations are perhaps better illustrated by considering linear elements, $k = 1$, for which an explicit expression for the correction can be readily obtained. Let $\boldsymbol{p} \in [\mathcal{P}_0(E)]^d$ and $v \in \mathcal{V}_1(E)$. Because $\boldsymbol{p}_v$ is constant over E and $\operatorname{div} \boldsymbol{p} \equiv 0$, we have from (19)

$$|E| \, \boldsymbol{p} \cdot \boldsymbol{p}_v = \fint_E \boldsymbol{p} \cdot \boldsymbol{p}_v \mathrm{d}\boldsymbol{x} = \oint_{\partial E} v \, (\boldsymbol{p} \cdot \boldsymbol{n}) \, \mathrm{d}\boldsymbol{s} - \fint_E \boldsymbol{p} \cdot \nabla v \mathrm{d}\boldsymbol{x} = \boldsymbol{p} \cdot \left(\oint_{\partial E} v \boldsymbol{n} \mathrm{d}\boldsymbol{s} - \fint_E \nabla v \mathrm{d}\boldsymbol{x} \right) \tag{20}$$

Using the fact that $\boldsymbol{p}$ is arbitrary, we arrive at the following expression for the corrected gradient:

$$\nabla_{E,1} v = \nabla v + \frac{1}{|E|} \left(\oint_{\partial E} v \boldsymbol{n} \mathrm{d}\boldsymbol{s} - \fint_E \nabla v \mathrm{d}\boldsymbol{x} \right) \tag{21}$$

We can see from this expression that the perturbation is a constant field proportional to the error in satisfying the identity $\int_E \nabla v \mathrm{d}\boldsymbol{x} = \int_{\partial E} v \boldsymbol{n} \mathrm{d}\boldsymbol{s}$ by the volumetric and surface quadrature schemes. It is worth noting that the requirement that the volumetric and surface quadratures exactly integrate constant and linear fields, respectively, implies that no error is incurred in the satisfaction of this

DOI: 10.1002/nme

identity whenever v is a linear field. This also implies that if $v \in \mathcal{P}_1(E)$, then there is no correction to its gradient, that is, $\nabla_{E,1} v = \nabla v$.

The latter observation in fact generalizes for any k. In particular,

$$\nabla_{E,k} q = \nabla q, \qquad \forall q \in \mathcal{P}_k(E) \tag{22}$$

which shows that the corrected gradient coincides with the exact gradient when applied to kth order polynomials. This can be seen by setting $\boldsymbol{p} = \nabla_{E,k} q - \nabla q = \boldsymbol{p}_q$ in (19) and using the exactness of the quadrature rules:

$$\begin{aligned} \int_E \left|\nabla_{E,k} q - \nabla q\right|^2 \mathrm{d}\boldsymbol{x} &= -\fint_E q \operatorname{div} \boldsymbol{p}_q \mathrm{d}\boldsymbol{x} + \oint_{\partial E} q(\boldsymbol{p}_q \cdot \boldsymbol{n}) \mathrm{d}s - \fint_E \boldsymbol{p}_q \cdot \nabla q \mathrm{d}\boldsymbol{x} \\ &= -\int_E q \operatorname{div} \boldsymbol{p}_q \mathrm{d}\boldsymbol{x} + \int_{\partial E} q(\boldsymbol{p}_q \cdot \boldsymbol{n}) \mathrm{d}s - \int_E \boldsymbol{p}_q \cdot \nabla q \mathrm{d}\boldsymbol{x} \\ &= 0 \end{aligned} \tag{23}$$

As we shall see in the next section, this property of the correction scheme plays an important role in ensuring that the resulting discretizations are polynomially consistent and satisfy the patch test.

Let us return to the corrected gradient (21) for linear elements, but now consider the two-dimensional setting wherein the variation of v on ∂E is piecewise linear and, as such, the boundary quadrature is exact. In this case, $\oint_{\partial E} v\boldsymbol{n} \mathrm{d}s = \int_{\partial E} v\boldsymbol{n} \mathrm{d}s = \int_E \nabla v \mathrm{d}\boldsymbol{x}$, and subsequently,

$$\nabla_{E,1} v = \nabla v + \frac{1}{|E|} \left(\int_E \nabla v \mathrm{d}\boldsymbol{x} - \fint_E \nabla v \mathrm{d}\boldsymbol{x} \right) \tag{24}$$

The perturbation is simply the difference between the volume average of ∇v and its approximations through the quadrature. A key observation immediate from (24) is that

$$\fint_E \nabla_{E,1} v \mathrm{d}\boldsymbol{x} = \int_E \nabla v \mathrm{d}\boldsymbol{x} \tag{25}$$

This shows that the corrected gradient $\nabla_{E,1} v$ under the action of the quadrature behaves like ∇v under exact integration. Because we are forced to use inexact integration when dealing with polygonal and polyhedral finite elements, we shall replace the gradient by its correction to offset the incurred error.

In the general case, it is expected from the definition of the correction that

$$\fint_E \boldsymbol{\psi} \cdot \nabla_{E,k} v \mathrm{d}\boldsymbol{x} - \int_E \boldsymbol{\psi} \cdot \nabla v \mathrm{d}\boldsymbol{x} = O(h_E^k) \left\|\nabla v\right\|_{L^2(E)^d} \tag{26}$$

for $v \in \mathcal{V}_k(E)$ and $\boldsymbol{\psi}$ a sufficiently smooth vector field. Here, h_E is the diameter of element E. This estimate will be used in the next section to show that replacing the gradient by its correction, when using quadrature, lowers the consistency error in the discretization to the same level as the approximation error. As such, optimal convergence rates are restored.

We end this section with an observation about the kernel of $\nabla_{E,k}$, namely that[‖]

$$\nabla_{E,k} v \equiv 0 \quad \Longrightarrow \quad \nabla v \equiv 0 \tag{27}$$

To see this, note that $\nabla_{E,k} v \equiv 0$ together with C1 imply that $\nabla v \in [\mathcal{P}_{k-1}(E)]^d$ and thus $v \in \mathcal{P}_k(E)$. From (22), we conclude that $\nabla v = \nabla_{E,k} v \equiv 0$. This indicates that spurious zero energy modes do not appear when using corrected gradients and thus can be useful in proving that the resulting discretization scheme inherits the stability characteristics of its Galerkin counterpart.

[‖]The converse is also true and follows immediately from (22).

DOI: 10.1002/nme

5. PROPOSED DISCRETIZATION SCHEME

We now discuss the use of gradient correction for the discretization of a general elliptic problem and illustrate how it can restore polynomial consistency that is otherwise lost in the presence of quadrature error. Let Ω be a smooth domain in $\mathbb{R}^d$, and consider the system of equations

$$-\operatorname{div}[\boldsymbol{a}(\boldsymbol{x}, u, \nabla u)] = f \text{ in } \Omega \tag{28}$$

$$u = g \text{ on } \partial\Omega \tag{29}$$

where the source function f and boundary data g are given fields with sufficient regularity. We recover the Poisson problem with the choice of $\boldsymbol{a}(\boldsymbol{x}, u, \boldsymbol{\xi}) = \boldsymbol{\xi}$, anisotropic linear diffusion by setting $\boldsymbol{a}(\boldsymbol{x}, u, \boldsymbol{\xi}) = \mathsf{K}(\boldsymbol{x})\boldsymbol{\xi}$, and Forchheimer flow with $\boldsymbol{a}(\boldsymbol{x}, u, \boldsymbol{\xi}) = 2\boldsymbol{\xi} / \left[1 + (1 + 4\beta\,|\boldsymbol{\xi}|)^{1/2}\right]$. Under suitable regularity assumptions on $\boldsymbol{a}$, the weak form of (28) and (29) consists of seeking $u \in H^1_g(\Omega) = \left\{v \in H^1(\Omega) : v|_{\partial\Omega} = g\right\}$ such that

$$\int_\Omega \boldsymbol{a}(\boldsymbol{x}, u, \nabla u) \cdot \nabla v \mathrm{d}\boldsymbol{x} = \int_\Omega f v \mathrm{d}\boldsymbol{x}, \qquad \forall v \in H^1_0(\Omega) \tag{30}$$

In order to define the finite element approximation of (30), consider a partition $\mathcal{T}_h$ of Ω consisting of non-overlapping strictly convex simple polyhedra with maximum diameter h. A conforming approximation space $\mathcal{V}_{h,k}$ associated with $\mathcal{T}_h$, based on the kth order element spaces defined in Section 2, is given by

$$\mathcal{V}_{h,k} = \left\{v \in C^0(\overline{\Omega}) : v_h|_E \in \mathcal{V}_k(E),\ \forall E \in \mathcal{T}_h\right\} \tag{31}$$

It is assumed that the elements in $\mathcal{T}_h$ satisfy suitable shape regularity requirements such that $\mathcal{V}_{h,k}$ yields optimal approximation estimates (refer to [19] for such conditions for two-dimensional and three-dimensional Wachspress functions). The set of functions in $\mathcal{V}_{h,k}$ whose trace on $\partial\Omega$ is equal to g will be denoted by $\mathcal{V}^g_{h,k}$.

We next define the quadrature over Ω that is given by the application of element quadrature rules. With a possible abuse of notation, we shall denote this quadrature by $\fint_\Omega$ and so, we have $\fint_\Omega = \sum_{E\in\mathcal{T}_h} \fint_E$. Similarly, we define a global discrete gradient map $\nabla_{h,k} : \mathcal{V}_{h,k} \to L^2(\Omega)^d$ such that over the elements of the mesh, it coincides with the corrected gradient defined in the last section. Therefore,

$$\nabla_{h,k} v|_E = \nabla_{E,k} v, \qquad \forall E \in \mathcal{T}_h \tag{32}$$

The proposed approximation using the space $\mathcal{V}_{h,k}$ would replace both instances of ∇ with the discrete gradient $\nabla_{h,k}$ along with the introduction of the quadrature. The approximate solution $u_h \in \mathcal{V}^g_{h,k}$ therefore satisfies

$$\fint_\Omega \boldsymbol{a}(\boldsymbol{x}, u, \nabla_{h,k} u_h) \cdot \nabla_{h,k} v \mathrm{d}\boldsymbol{x} = \fint_\Omega f v \mathrm{d}\boldsymbol{x}, \qquad \forall v \in \mathcal{V}^0_{h,k} \tag{33}$$

In practice, this amounts to simply using the corrected gradient of the basis functions when integrating with the weak form along with the associated quadrature rules.

To assess the consistency of approximation, we consider the so-called patch test that refers to the case where the exact solution is a polynomial field, that is, $u = p \in \mathcal{P}_k(\Omega)$. The problem data is accordingly given by $f = -\operatorname{div}\boldsymbol{a}(\boldsymbol{x}, u, \nabla p)$ and $g = p|_{\partial\Omega}$.

We begin by showing that the patch test is passed *exactly*, that is, $u_h = p$, for linear diffusion $\boldsymbol{a}(\boldsymbol{x}, u, \boldsymbol{\xi}) = \mathsf{K}\boldsymbol{\xi}$ with constant tensor K. By the polynomial precision of the local spaces, $\mathcal{P}_k(\Omega) \subseteq \mathcal{V}^g_{h,k}$ and so $u_h = p \in \mathcal{V}^g_{h,k}$. Moreover, it follows from (22) that

$$\nabla_{h,k} u_h = \nabla_{h,k} p = \nabla p \tag{34}$$

DOI: 10.1002/nme

In order to verify (33), we consider an arbitrary test function $v \in \mathcal{V}^0_{h,k}$. We have

$$\begin{aligned}
\fint_\Omega \mathsf{K}\nabla_{h,k}u_h \cdot \nabla_{h,k} v \mathrm{d}\boldsymbol{x} &= \sum_{E\in\mathcal{T}_h} \fint_E \mathsf{K}\nabla p \cdot \nabla_{E,k} v \mathrm{d}\boldsymbol{x} \\
&= \sum_{E\in\mathcal{T}_h} \left[-\fint_E v \,\mathrm{div}\,(\mathsf{K}\nabla p)\,\mathrm{d}\boldsymbol{x} + \oint_{\partial E} v\,(\mathsf{K}\nabla p\cdot\boldsymbol{n})\,\mathrm{d}\boldsymbol{s}\right] \qquad (35)\\
&= \fint_\Omega f v \mathrm{d}\boldsymbol{x}
\end{aligned}$$

In the second equality, we have used the definition of $\nabla_{E,k}$ and the fact that $\mathsf{K}\nabla p|_E \in [\mathcal{P}_{k-1}(E)]^d$. Note that the second term in (35) vanishes as the internal edges of the mesh are visited twice (the normal vector $\boldsymbol{n}$ changes sign each time) and $v = 0$ on the boundary edges. Our numerical studies presented in Section 7 confirm that the patch test will be passed up to machine precision errors.

For a general function $\boldsymbol{a}$, $u_h = p$ may not exactly satisfy (33) though the remainder is expected to be $O(h^k)$. Assuming sufficiently regularity of $\boldsymbol{a}$, we have

$$\begin{aligned}
\fint_\Omega \boldsymbol{a}(\boldsymbol{x}, p, \nabla p)\cdot\nabla_{h,k} v \mathrm{d}\boldsymbol{x} - \fint_\Omega f v \mathrm{d}\boldsymbol{x} &= \int_\Omega \boldsymbol{a}(\boldsymbol{x}, p, \nabla p)\cdot\nabla v \mathrm{d}\boldsymbol{x} + O(h^k)\|\nabla v\|_{L^2(\Omega)^d} - \fint_\Omega f v \mathrm{d}\boldsymbol{x} \\
&= \int_\Omega f v \mathrm{d}\boldsymbol{x} + O(h^k)\,\|\nabla v\|_{L^2(\Omega)^d} - \fint_\Omega f v \mathrm{d}\boldsymbol{x} \\
&= O(h^k)\,\|\nabla v\|_{L^2(\Omega)^d}
\end{aligned} \qquad (36)$$

The first equality is a consequence of estimate (26), and the last one comes from the accuracy of the volumetric quadrature and smoothness of f. This bound for the consistency error (the error in the satisfaction of the discrete problem by the exact solution) suggests that the patch test will be passed asymptotically with mesh refinement at the optimal rate of k.

While a rigorous error analysis[**] is beyond the scope of this work, let us briefly discuss the general case where the exact solution u is a sufficiently smooth field. The consistency error resulting from the combined effects of using quadrature and replacing ∇ with $\nabla_{h,k}$ can be decomposed into two parts[††]:

$$\begin{aligned}
&\fint_\Omega \boldsymbol{a}(\boldsymbol{x}, u, \nabla_{h,k}u)\cdot\nabla_{h,k} v \mathrm{d}\boldsymbol{x} \\
&\qquad - \fint_\Omega f v \mathrm{d}\boldsymbol{x} = \left[\fint_\Omega \boldsymbol{a}(\boldsymbol{x}, u, \nabla u)\cdot\nabla_{h,k} v \mathrm{d}\boldsymbol{x} - \fint_\Omega f v \mathrm{d}\boldsymbol{x}\right] \qquad (37)\\
&\qquad\qquad + \fint_\Omega \left[\boldsymbol{a}(\boldsymbol{x}, u, \nabla_{h,k}u) - \boldsymbol{a}(\boldsymbol{x}, u, \nabla u)\right]\cdot\nabla_{h,k} v \mathrm{d}\boldsymbol{x}
\end{aligned}$$

We can show that the term in the bracket is $O(h^k)\,\|\nabla v\|_{L^2(\Omega)^d}$ in a similar way as (36). That the second error term is of the same order is, roughly speaking, a consequence of (22) and regularity of $\boldsymbol{a}$.

This discussion also suggests that a non-symmetric discretization featuring

$$\fint_\Omega \boldsymbol{a}(\boldsymbol{x}, u, \nabla u)\cdot\nabla_{h,k} v \mathrm{d}\boldsymbol{x} \qquad (38)$$

in left hand side of (33) leads to optimally convergent approximations. While our preliminary numerical results in fact confirm this, we have elected not to further discuss this approach since it is of less practical use compared with the symmetric scheme.

[**]This should also include an analysis of the stability of the proposed discretization scheme.

[††]While the corrected gradient $\nabla_{E,k}$ was defined for elements of $\mathcal{V}_k(E)$, its definition can be readily extended to sufficiently smooth functions in $\boldsymbol{H}^1(E)$ for which the quadrature makes sense. The properties of corrected gradient discussed in the last section will continue to hold.

DOI: 10.1002/nme

6. COMPARISON WITH EXISTING METHODS

We begin this section by comparing the present gradient correction scheme for linear polyhedra with the pseudo-derivative construction of [11]. To describe this approach, we will denote by $\{(\boldsymbol{x}_q, w_q) : q = 1, \dots, Q\}$ the set of quadrature points and weights for $\fint_E$. As discussed in [12] in the context of polyhedral finite elements, the pseudo-derivative of $v \in \mathcal{V}_1(E)$ at $\boldsymbol{x}_q$, denoted by $\boldsymbol{\xi}_q^v$, is determined by solving the following constrained minimization problem:

$$\min_{\boldsymbol{\xi}_1,\dots,\boldsymbol{\xi}_Q} \sum_{q=1}^{Q} \left|\nabla v(\boldsymbol{x}_q) - \boldsymbol{\xi}_q\right|^2 \quad \text{subject to} \quad \sum_{q=1}^{Q} w_q \boldsymbol{\xi}_q = \oint_{\partial E} v\boldsymbol{n}\mathrm{d}\boldsymbol{s} \tag{39}$$

The explicit solution to this problem is given by

$$\begin{aligned} \boldsymbol{\xi}_q^v &= \nabla v(\boldsymbol{x}_q) + \frac{w_q}{\sum_{t=1}^{Q} w_t^2}\left[\oint_{\partial E} v\boldsymbol{n}\mathrm{d}\boldsymbol{s} - \sum_{t=1}^{Q} w_t \nabla v(\boldsymbol{x}_t)\right] \\ &= \nabla v(\boldsymbol{x}_q) + \frac{w_q}{\sum_{t=1}^{Q} w_t^2}\left(\oint_{\partial E} v\boldsymbol{n}\mathrm{d}\boldsymbol{s} - \fint_E \nabla v \mathrm{d}\boldsymbol{x}\right), \qquad q = 1, \dots, Q \end{aligned} \tag{40}$$

The difference between the pseudo-derivative and the corrected gradient defined via (12) and (13) lies in the choice of the objective function. Observe that the objective function in (12) can be written as

$$\fint_E |\nabla v - \boldsymbol{\xi}|^2 \,\mathrm{d}\boldsymbol{x} = \sum_{q=1}^{Q} w_q \left|\nabla v(\boldsymbol{x}_q) - \boldsymbol{\xi}(\boldsymbol{x}_q)\right|^2 \tag{41}$$

which compared with (39) features a reasonable scaling by the quadrature weights.

Whereas the pseudo-derivative is only defined at the quadrature points, the corrected gradient $\nabla_{E,1} v$ is field over all of E. Moreover, the perturbation $\nabla_{E,1} v - \nabla v$ is constant over E and, as such, takes the same value for all $\boldsymbol{x}_q$. By contrast, it can be seen from (40) that the difference $\boldsymbol{\xi}_q^v - \nabla v(\boldsymbol{x}_q)$ involves a particular scaling of the same constant by the quadrature weights.

The differences between the pseudo-derivatives and present corrected gradients are more pronounced for higher order elements. The pseudo-derivative construction in such cases (see, for example, [21]) masks the nature of perturbation needed to restore the consistency of the gradient field in the presence of quadrature error.

We next compare the present approach with the scheme proposed in [6, 7] for first-order polygons. Because that approach is only applicable to linear PDEs (at least at the present level of development), we consider the case $\boldsymbol{a}(x, u, \boldsymbol{\xi}) = \mathsf{K}\boldsymbol{\xi}$ where K is a constant tensor over each element in the mesh.

Let us recall the definition of local projection map π_E used in [6] and originally proposed in [8]: given $v \in \mathcal{V}_1(E)$, $\pi_E v$ is its projection on $\mathcal{P}_1(E)$ such that

$$\nabla \pi_E v = \frac{1}{|E|}\int_E \nabla v \mathrm{d}\boldsymbol{x} \tag{42}$$

Note that this quantity can be computed exactly using the identity $\int_E \nabla v \mathrm{d}\boldsymbol{x} = \int_{\partial E} v\boldsymbol{n}\mathrm{d}s$ and the fact that v is piecewise linear on ∂E. From this, it follows that the exact energy has the following decomposition:

$$\int_\Omega \mathsf{K}\nabla u \cdot \nabla v \mathrm{d}\boldsymbol{x} = \sum_{E\in\mathcal{T}_h}\left[\int_E \mathsf{K}\nabla\pi_E u \cdot \nabla \pi_E v \mathrm{d}\boldsymbol{x} + \int_E \mathsf{K}\nabla\left(u - \pi_E u\right)\cdot\nabla\left(v - \pi_E v\right)\mathrm{d}\boldsymbol{x}\right] \tag{43}$$

DOI: 10.1002/nme

To remove the consistency error present in $\fint_\Omega \mathsf{K}\nabla u \cdot \nabla v \mathrm{d}\boldsymbol{x}$, it is proposed to apply quadrature to the right-hand-side expansion and use the following approximation to the energy bilinear form

$$\sum_{E\in\mathcal{T}_h}\left[\int_E \mathsf{K}\nabla\pi_E u\cdot\nabla\pi_E v\mathrm{d}\boldsymbol{x} + \fint_E \mathsf{K}\nabla\left(u-\pi_E u\right)\cdot\nabla\left(v-\pi_E v\right)\mathrm{d}\boldsymbol{x}\right] \tag{44}$$

Observe that the first term is integrated exactly given the precision of the quadrature rule.

In order to connect this approach to the present one, let us define another local projection onto $\mathcal{P}_1(E)$, denoted by τ_E, such that for $v\in\mathcal{V}_1(E)$,

$$\nabla\tau_E v = \frac{1}{|E|}\fint_E \nabla v\mathrm{d}\boldsymbol{x} \tag{45}$$

Note that the different between π_E and τ_E lies in the use of quadrature in the latter.

We can see from (24) that the corrected gradient can be written as

$$\nabla_{E,1}v = \nabla\left(v+\pi_E v-\tau_E v\right) \tag{46}$$

Using this, we expand the approximation to the energy bilinear form in (33):

$$\begin{aligned}\fint_\Omega \mathsf{K}\nabla_{h,1}u\cdot\nabla_{h,1}v\mathrm{d}\boldsymbol{x} &= \sum_{E\in\mathcal{T}_h}\fint_E \mathsf{K}\nabla\left(u+\pi_E u-\tau_E u\right)\cdot\nabla\left(v+\pi_E v-\tau_E v\right)\mathrm{d}\boldsymbol{x}\\ &= \sum_{E\in\mathcal{T}_h}\left[\int_E \mathsf{K}\nabla\pi_E u\cdot\nabla\pi_E v\mathrm{d}\boldsymbol{x} + \fint_E \mathsf{K}\nabla\left(u-\tau_E u\right)\cdot\nabla\left(v-\tau_E v\right)\mathrm{d}\boldsymbol{x}\right]\end{aligned} \tag{47}$$

In the second equality, we have used the fact that the two cross terms vanish:

$$\fint_E \mathsf{K}\nabla\pi_E u\cdot\nabla\left(v-\tau_E v\right)\mathrm{d}\boldsymbol{x} = \fint_E \mathsf{K}\nabla\left(u-\tau_E u\right)\cdot\nabla\pi_E v\mathrm{d}\boldsymbol{x} = 0 \tag{48}$$

This follows from the definition of τ_E.

Comparing (44) and (47), we can see that the first term, which is responsible for the polynomial consistency of the local energy, is identical in both expansions. The only difference between them lies in the appearance of τ_E in place of π_E in the second term. The second term in both cases vanishes if u is a linear polynomial. Moreover, it is worth noting that the difference between the two energies is given by

$$\sum_{E\in\mathcal{T}_h}\fint_E \mathsf{K}\nabla\left(\pi_E u-\tau_E u\right)\cdot\nabla\left(\pi_E v-\tau_E v\right)\mathrm{d}\boldsymbol{x} = \sum_{E\in\mathcal{T}_h}\int_E \mathsf{K}\left(\nabla_{E,1}u-\nabla u\right)\cdot\left(\nabla_{E,1}v-\nabla v\right)\mathrm{d}\boldsymbol{x} \tag{49}$$

which is the exact energy associated with the perturbations defining the corrected gradient.

As noted before, the main limitation of the proposed scheme in [6] is that it is applicable only to linear problems for which the energy bilinear form can be decomposed into its polynomial and non-polynomial parts through the use of projection maps π_E. The gradient correction approach, however, treats linear and nonlinear problems in the same manner.

7. NUMERICAL STUDIES

In this section, we present results for several numerical examples assessing the performance of the proposed correction scheme for the general model problem (28) and (29). The example problems, posed on the unit square or cube $\Omega=(0,1)^d$, have known analytical solutions and are solved using meshes shown in Figures 2–5. In Tables I and II, the various mesh parameters are presented (h is

DOI: 10.1002/nme

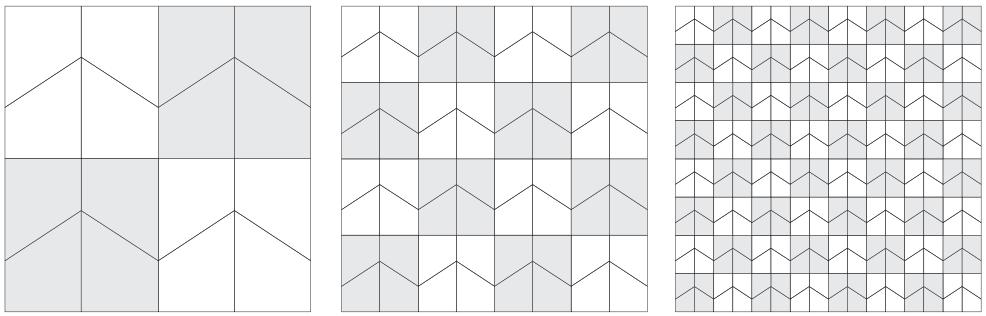

Figure 2. Representative examples of trapezoidals meshes. Three consecutive meshes are shown, containing 16, 64, and 256 distorted quadrilaterals, respectively.

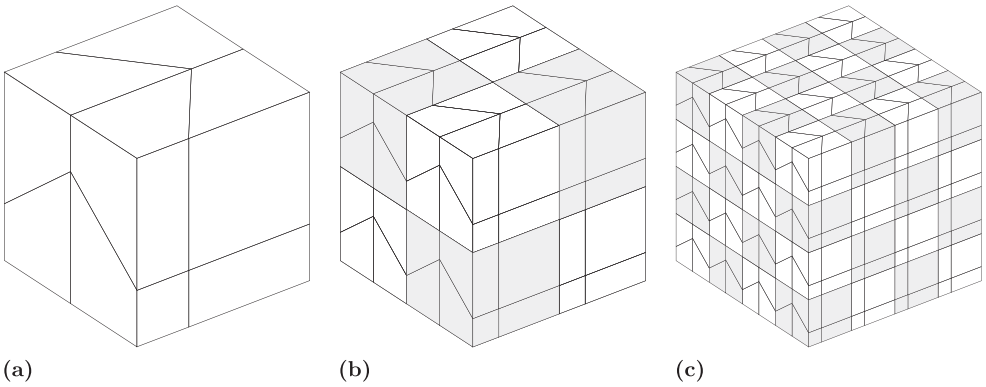

Figure 3. Representative examples of distorted hexahedral mesh. Three consecutive meshes are shown, containing 8, 64, and 512 distorted hexahedrons, respectively.

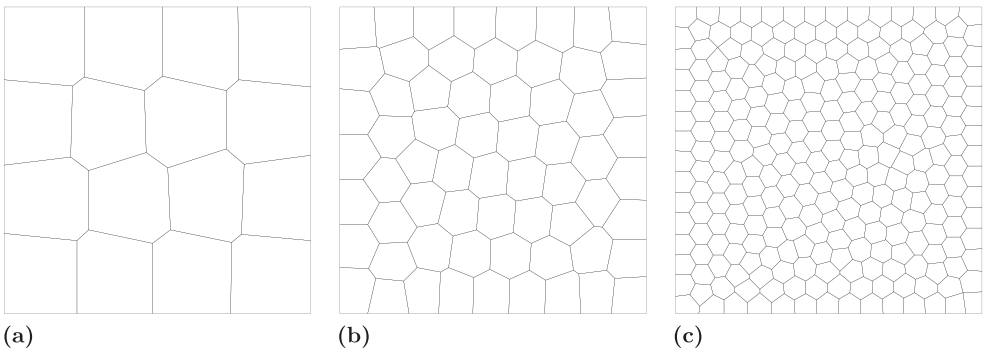

Figure 4. Representative examples of two-dimensional Voronoi mesh. Three consecutive meshes are shown, containing 16, 64, and 256 polygons, respectively.

the maximum diameter of the elements in the mesh). The boundary data g and source functions f are prescribed in accordance with the exact solution u. Note that for the trapezoidal and distorted hexahedral meshes, the Wachspress functions are different from the commonly used iso-parametric bilinear and trilinear basis functions. Unless otherwise stated, the volumetric and surface quadrature rules underlying the discretization are those described in Section 3. The accuracy and convergence of the proposed discretization (33) is determined through two global measures of error, namely the L^2-error $\|u - u_h\|_{L^2(\Omega)}$ and the H^1-semi-norm $\|\nabla u - \nabla u_h\|_{L^2(\Omega)^d}$ that are computed using a fifth-order rule on simplicial partition of the mesh. In addition to the proposed scheme, we also

DOI: 10.1002/nme

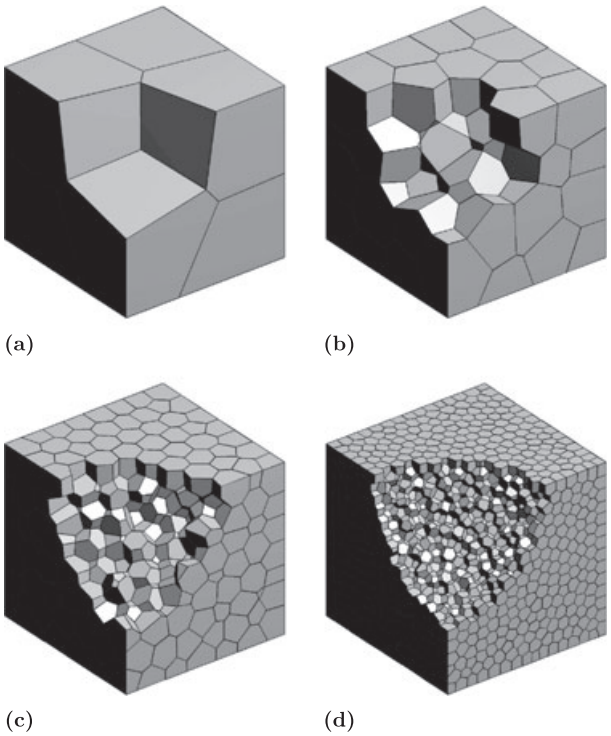

Figure 5. Representative examples of three-dimensional centroidal Voronoi mesh. A portion of each mesh has been removed to show the internal structure.

Table I. Statistics for two-dimensional meshes.

		Number of nodes		Mesh size h	
Mesh	Number of elements	Trapezoidal	Voronoi	Trapezoidal	Voronoi
a	16	25	34	0.41667	0.35447
b	64	81	130	0.20833	0.18427
c	256	289	512	0.10417	0.09683
d	1024	1089	2047	0.05208	0.04737
e	4096	4225	8172	0.02604	0.02454
f	16,384	16,641	32,721	0.01302	0.01157
g	65,536	66,049	130,822	0.00651	0.00592

Table II. Statistics for three-dimensional meshes.

		Number of nodes		Mesh size h	
Mesh	Number of elements	Distorted hexahedral	Voronoi	Distorted hexahedral	Voronoi
a	8	27	38	1.10905	0.90198
b	64	125	327	0.55453	0.48074
c	512	729	2798	0.27726	0.24666
d	4096	4913	23,226	0.13863	0.12274
e	32,768	35,937	190,078	0.06932	0.06095

provide the results for the approximation using quadrature but without correction of the gradient defined by what follows:

$$\text{Find } u_h \in \mathcal{V}_{h,k}^g \text{ such that } \quad \fint_\Omega \boldsymbol{a}(\boldsymbol{x}, u, \nabla u_h) \cdot \nabla v \mathrm{d}\boldsymbol{x} = \fint_\Omega f v \mathrm{d}\boldsymbol{x}, \quad \forall v \in \mathcal{V}_{h,k}^0 \tag{50}$$

DOI: 10.1002/nme

and for the Galerkin approximation with exact integration as follows:

$$\text{Find } u_h \in \mathcal{V}^g_{h,k} \text{ such that } \quad \int_\Omega \boldsymbol{a}(\boldsymbol{x}, u, \nabla u_h) \cdot \nabla v \mathrm{d}\boldsymbol{x} = \int_\Omega f v \mathrm{d}\boldsymbol{x}, \quad \forall v \in \mathcal{V}^0_{h,k} \tag{51}$$

As a surrogate for the latter, we use (33) and the aforementioned fifth-order rule. We have observed that increasing the order of integration beyond this has little effect on the resulting errors. The results labeled 'exact' in Figures 6–11 represent the Galerkin errors and are obtained using this approach. The Galerkin error, which is a function of the approximation capability of the finite element spaces, serves as a reference to determine the extent to which the integration error resulting from 'minimal' quadrature rules influences the accuracy.

We begin with a patch test study for the Poisson problem, $\boldsymbol{a}(x, u, \boldsymbol{\xi}) = \boldsymbol{\xi}$, to verify the analysis of Section 5. The results using the Voronoi meshes are summarized in Table III. For the two-dimensional case, the exact solution is set to $u(\boldsymbol{x}) = x - y$ for linear and $u(\boldsymbol{x}) = x^2 - 2xy + 4y$ for quadratic discretizations. In the three-dimensional case, the exact solution is chosen as $u(\boldsymbol{x}) = x + 2y + 3z$. We can see from the numerical results for the correction scheme that the errors are at machine precisions levels though they evidently accumulate with mesh refinement. For the next set of numerical results, we solve benchmark linear anisotropic diffusion problems, with $\boldsymbol{a}(x, u, \boldsymbol{\xi}) = \mathsf{K}(\boldsymbol{x})\boldsymbol{\xi}$. Borrowing from [22], we consider the two-dimensional problem with the exact

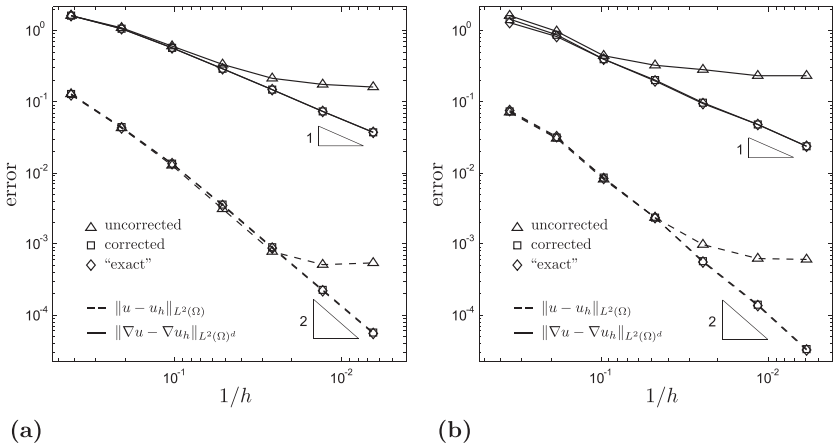

Figure 6. Results of the convergence study for the two-dimensional anisotropic diffusion problem with first-order finite elements on (a) trapezoidal (b) Voronoi meshes.

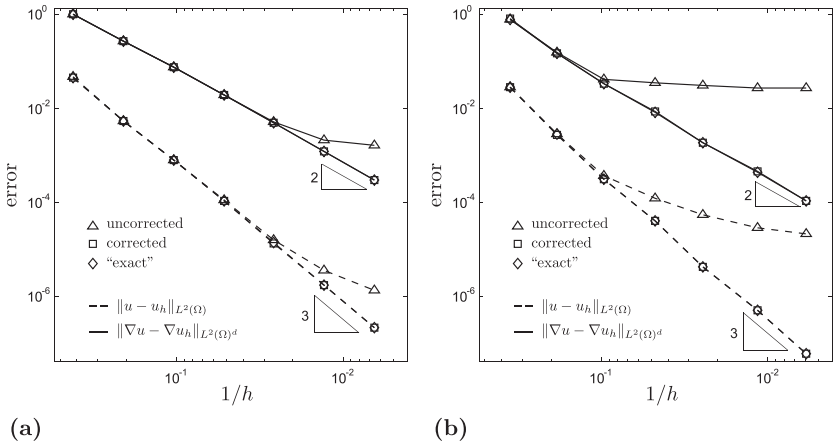

Figure 7. Results of the convergence study for the two-dimensional anisotropic diffusion problem with second-order finite elements on (a) trapezoidal (b) Voronoi meshes.

DOI: 10.1002/nme

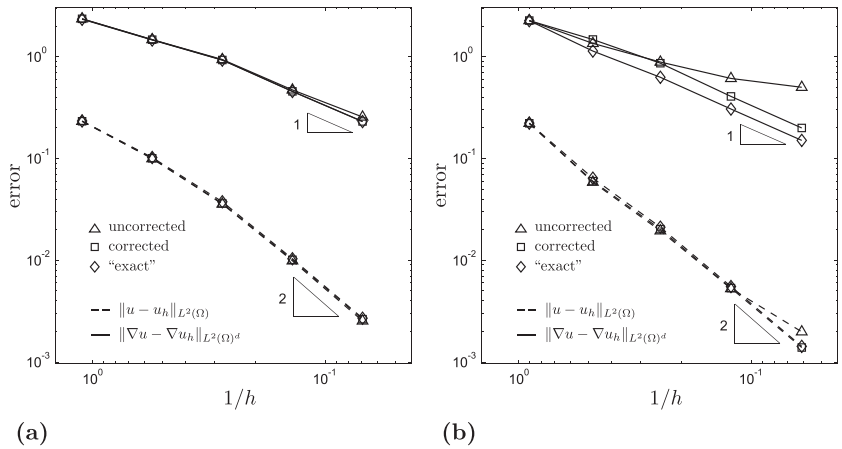

Figure 8. Results of the convergence study for the three-dimensional anisotropic diffusion problem with first-order finite elements on (a) trapezoidal (b) Voronoi meshes.

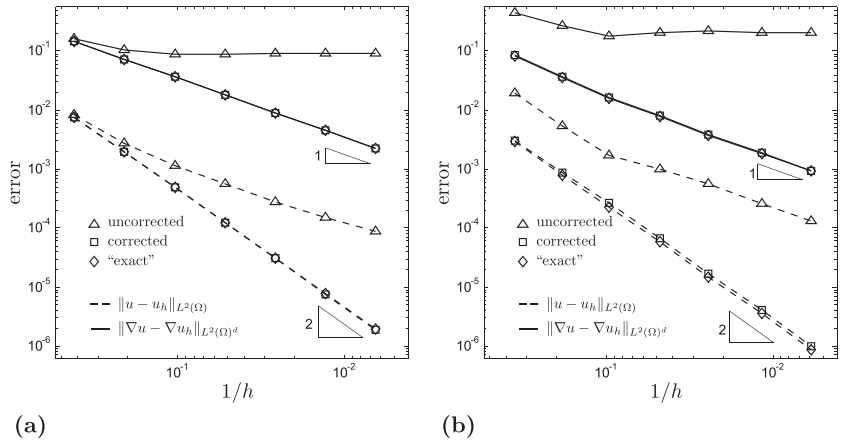

Figure 9. Results of the convergence study for the two-dimensional Forchheimer flow problem with first-order order finite elements on (a) trapezoidal (b) Voronoi meshes.

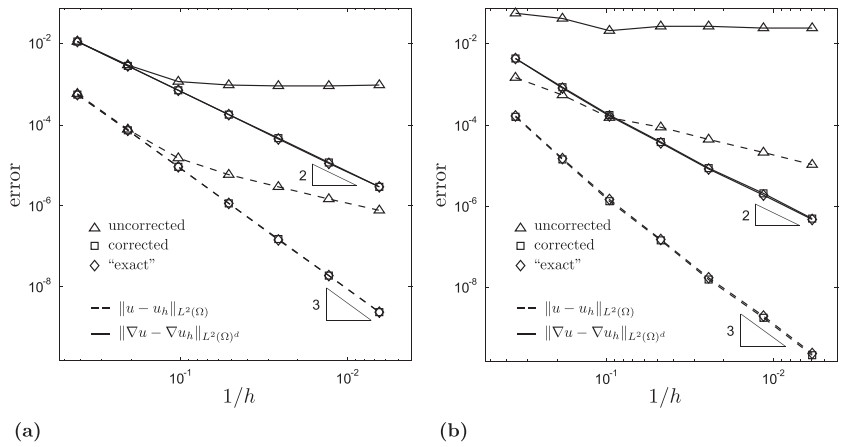

Figure 10. Results of the convergence study for the two-dimensional Forchheimer flow problem with second-order finite elements on (a) trapezoidal (b) Voronoi meshes.

DOI: 10.1002/nme

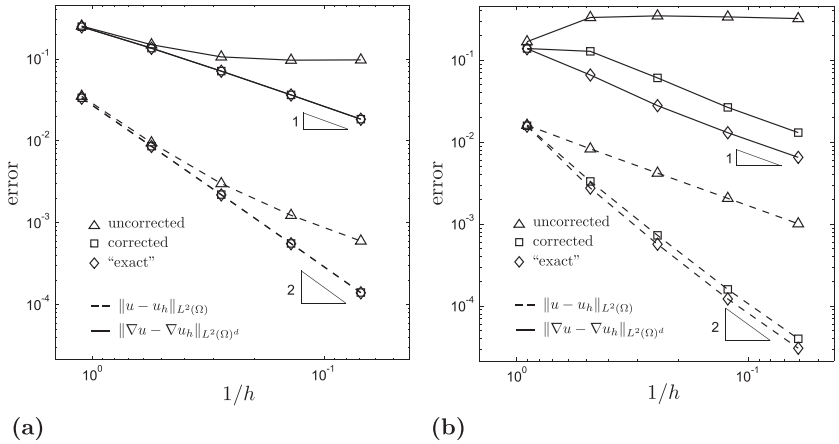

Figure 11. Results of the convergence study for the three-dimensional Forchheimer flow problem with first-order finite elements on (a) trapezoidal (b) Voronoi meshes.

Table III. H^1-error for the patch test performed on two-dimensional and three-dimensional Voronoi meshes.

	Two-dimensional				Three-dimensional	
	Linear		Quadratic		Linear	
Mesh	Corrected	Uncorrected	Corrected	Uncorrected	Corrected	Uncorrected
a	3.358E-15	1.292E-01	3.509E-13	5.669E-02	3.136E-12	2.678E-01
b	7.504E-15	1.930E-01	7.663E-13	5.885E-02	8.184E-12	7.122E-01
c	1.287E-14	1.018E-01	2.395E-12	3.359E-02	2.585E-11	8.097E-01
d	2.585E-14	1.310E-01	1.483E-11	3.892E-02	1.751E-11	7.349E-01
e	5.045E-14	1.235E-01	1.203E-10	3.563E-02	8.553E-09	7.206E-01

solution and diffusion tensor given by

$$u(\boldsymbol{x}) = x_1^3 x_2^2 + x_1 \sin(2\pi x_1 x_2)\sin(2\pi x_2), \qquad \mathsf{K}(\boldsymbol{x}) = \begin{bmatrix} (x_1+1)^2 + x_2^2 & -x_1 x_2 \\ -x_1 x_2 & (x_1+1)^2 \end{bmatrix} \tag{52}$$

For the three-dimensional study, we solve the problem defined by

$$u(\boldsymbol{x}) = x_1^3 x_2^2 x_3 + x_1 \sin(2\pi x_1 x_2)\sin(2\pi x_2)\sin(2\pi x_3) \tag{53}$$

$$\mathsf{K}(\boldsymbol{x}) = \begin{bmatrix} x_2^2 + x_3^2 + 1 & -x_1 x_2 & -x_1 x_3 \\ -x_1 x_2 & x_1^2 + x_3^2 + 1 & -x_2 x_3 \\ -x_1 x_3 & -x_2 x_3 & x_1^2 + x_2^2 + 1 \end{bmatrix} \tag{54}$$

The results for linear and quadratic discretizations (latter only in two dimensions) and different mesh types are summarized in Figures 6–8. Consistent with the observations in [6], we can see a degradation of convergence rates and eventually lack of convergence of approximations without the use of corrected gradient. The source of this behavior must be attributed to integration error because the Galerkin approximation is optimally convergent. For the results with quadratic finite elements, the onset of degraded convergence occurs for coarser meshes compared with linear elements because the approximation error decays more quickly and, as such, the consistency error dominates earlier. This is more noticeable for Voronoi meshes where we anticipate the integration error and subsequently, in the absence of correction, the consistency error to be larger. With the correction of gradient, not only are the optimal convergence rates restored, but also the errors levels are nearly

DOI: 10.1002/nme

identical to the Galerkin errors. Viewed another way, increasing the order of integration has negligible effect on the errors levels once the polynomial consistency errors are controlled. This is promising from the point of view of computational cost because the quadrature rules of Section 3 respecting the minimal accuracy requirements demand only a modest number of integration points.

We conclude this section with results for the nonlinear Forchheimer flow defined by

$$\boldsymbol{a}(\boldsymbol{x}, u, \boldsymbol{\xi}) = \frac{2\boldsymbol{\xi}}{1 + \sqrt{1 + 4\beta\,|\boldsymbol{\xi}|}} \tag{55}$$

The value of $\beta = 40$ is selected along with exact solutions $u(\boldsymbol{x}) = \sin x_1 e^{x_2}$ and $u(\boldsymbol{x}) = x_3 \sin x_1 e^{x_2}$ for two-dimensional and three-dimensional problems, respectively. The resulting nonlinear algebraic system of equations are solved using the Newton–Rhapson method with line search. Figures 9–11 show the results for different approximation orders and mesh types.

We observe the same trends as the linear diffusion problem. The loss of accuracy without the correction of the gradient is even more severe for the nonlinear problem, which is particularly evident for Voronoi meshes. The correction scheme again delivers optimally convergent solutions with accuracy on par with the Galerkin approximations. This is noteworthy as it illustrates that accurate modeling of three-dimensional nonlinear problems with polyhedral finite elements is computationally feasible. For such problems, the overhead associated with computing shape function gradients and their corrections, compared with classical finite elements, is less significant because such computations need to be carried out only once. The correction scheme brings the computational cost of polygonal and polyhedral finite elements closer to that of the classical finite elements.

8. FUTURE WORK

As mentioned before, the development of second-order polyhedral finite elements, following the construction of [16], and the application of the correction scheme merits a separate study. Of particular interest is the construction of efficient volumetric and boundary quadrature rules, similar to vertex-based rules described here for the linear polyhedra, that respect the accuracy requirements for the gradient correction. Future work also includes the application of the gradient correction scheme for finite element approximation of other boundary values problems such as finite elasticity and Navier–Stokes equations.

ACKNOWLEDGEMENTS

We are thankful to the support from the US National Science Foundation (NSF) under grant CMMI 1437535. Ivan F. M. Menezes and Anderson Pereira acknowledge the financial support provided by Tecgraf/PUC-Rio (Group of Technology in Computer Graphics), Rio de Janeiro, Brazil. Any opinion, finding, conclusions, or recommendations expressed here are those of the authors and do not necessarily reflect the views of the sponsors.

APPENDIX

We provide details on the computation of the corrected gradient $\nabla_{E,k}$ of the basis functions with a unified treatment for both linear and quadratic elements. Let $\{\varphi_1, \ldots, \varphi_{n_\mathcal{V}}\}$ be the canonical basis for $\mathcal{V}_k(E)$ and $\{\boldsymbol{p}_1, \ldots, \boldsymbol{p}_{n_\mathcal{P}}\}$ a basis for $[\mathcal{P}_{k-1}(E)]^d$. By condition C1 (Section 4), there exists an $n_\mathcal{V} \times n_\mathcal{P}$ coefficients matrix $\boldsymbol{C}$ such that

$$\nabla_{E,k}\varphi_i = \nabla\varphi_i + \sum_{\alpha=1}^{n_\mathcal{P}} C_{i,\alpha}\boldsymbol{p}_\alpha, \qquad i = 1, \ldots, n_\mathcal{V} \tag{A.1}$$

DOI: 10.1002/nme

We compute an $n_{\mathcal{V}} \times n_{\mathcal{P}}$ matrix $\boldsymbol{R}$ and $n_{\mathcal{P}} \times n_{\mathcal{P}}$ matrix $\boldsymbol{K}$ with the following entries:

$$R_{i,\beta} = -\fint_E \nabla\varphi_i \cdot \boldsymbol{p}_\beta \mathrm{d}\boldsymbol{x} - \fint_E \varphi_i \operatorname{div} \boldsymbol{p}_\beta \mathrm{d}\boldsymbol{x} + \oint_{\partial E} \varphi_i (\boldsymbol{p}_\beta \cdot \boldsymbol{n}) \mathrm{d}\boldsymbol{s} \tag{A.2}$$

$$K_{\alpha,\beta} = \fint_E \boldsymbol{p}_\alpha \cdot \boldsymbol{p}_\beta \mathrm{d}\boldsymbol{x} \tag{A.3}$$

Note again that the integral in definition of $\boldsymbol{K}$ is computed exact because of the required precision of the volumetric quadrature. As such, one can readily see that $\boldsymbol{K}$ is a symmetric positive definite matrix.

Setting $v = \varphi_i$ and $\boldsymbol{p} = \boldsymbol{p}_\beta$ in (17) yields the following linear system of equations:

$$\sum_{\alpha=1}^{n_{\mathcal{P}}} C_{i,\alpha} K_{\alpha,\beta} = R_{i,\beta}, \qquad \beta = 1, \ldots, n_{\mathcal{P}} \tag{A.4}$$

Hence, the coefficient matrix is simply given by $\boldsymbol{C} = \boldsymbol{R}\boldsymbol{K}^{-1}$.

In practice, a non-intrusive implementation would involve calculation of the coefficient matrix $\boldsymbol{C}$ at the same routine where the basis functions are computed. Using (A.1), the corrected gradient would be computed (and, in the case of nonlinear problems, stored) at the location of the quadrature points and passed to the analysis code in place of the original basis function gradients.

REFERENCES

1. Sukumar N, Malsch EA. Recent advances in the construction of polygonal finite element interpolants. *Archives of Computational Methods in Engineering* 2006; **13**:129–163.
2. Talischi C, Paulino GH, Pereira A, Menezes IFM. PolyTop: a MATLAB implementation of a general topology optimization framework using unstructured polygonal finite element meshes. *Structural and Multidisciplinary Optimization* 2012; **45**:329–357.
3. Bishop JE. Simulating the pervasive fracture of materials and structures using randomly close packed Voronoi tessellations. *Computational Mechanics* 2009; **44**:455–471.
4. Leon SE, Spring DW, Paulino GH. Reduction in mesh bias for dynamic fracture using adaptive splitting of polygonal finite elements. *International Journal for Numerical Methods in Engineering* 2014; **100**:555–576.
5. Talischi C, Pereira A, Paulino GH, Menezes IFM, Carvalho MS. Polygonal finite elements for incompressible fluid flow. *International Journal for Numerical Methods in Fluids* 2014; **74**:134–151.
6. Talischi C, Paulino GH. Addressing integration error for polygonal finite elements through polynomial projections: a patch test connection. *Mathematical Models and Methods in Applied Sciences* 2014; **24**:1701–1727.
7. Manzini G, Russo A, Sukumar N. New perspectives on polygonal and polyhedral finite element methods. *Mathematical Models and Methods in Applied Sciences* 2014; **24**:1665–1699.
8. Beirão Da Veiga L, Brezzi F, Cangiani A, Manzini G, Marini LD, Russo A. Basic principles of virtual element methods. *Mathematical Models and Methods in Applied Sciences* 2013; **23**:199–214.
9. Beirão Da Veiga L, Brezzi F, Marini LD. Virtual elements for linear elasticity problems. *SIAM Journal on Numerical Analysis* 2013; **51**:794–812.
10. Brezzi F, Falk RS, Donatella Marini L. Basic principles of mixed virtual element methods. *ESAIM: Mathematical Modelling and Numerical Analysis* 2014; **48**:1227–1240.
11. Krongauz K, Belytschko TB. Consistent pseudo-derivatives in meshless methods. *Computer Methods in Applied Mechanics and Engineering* 1997; **146**:371–386.
12. Bishop JE. A displacement-based finite element formulation for general polyhedra using harmonic shape functions. *International Journal for Numerical Methods in Engineering* 2014; **97**:1–31.
13. Sukumar N. Quadratic maximum-entropy serendipity shape functions for arbitrary planar polygons. *Computer Methods in Applied Mechanics and Engineering* 2013; **263**:27–41.
14. Droniou J, Eymard R, Gallouet T, Herbin R. Gradient schemes: a generic framework for the discretisation of linear, nonlinear and nonlocal elliptic and parabolic equations. *Mathematical Models and Methods in Applied Sciences* 2013; **23**:2395–2432.
15. Floater MS, Hormann K, Kòs G. A general construction of barycentric coordinates over convex polygons. *Advances in Computational Mathematics* 2006; **24**:311–331.
16. Rand A, Gillette A, Bajaj C. Quadratic serendipity finite elements on polygons using generalized barycentric coordinates. *Mathematics of Computation* 2014; **83**:2691–2716.
17. Wachspress EL. *A Rational Finite Element Basis*. Academic Press: New York, 1975.

DOI: 10.1002/nme

18. Warren J, Schaefer S, Hirani AN, Desbrun M. Barycentric coordinates for convex sets. *Advances in Computational Mathematics* 2007; **27**:319–338.
19. Floater M, Gillette A, Sukumar N. Gradient bounds for Wachspress coordinates on polytopes. *SIAM Journal on Numerical Analysis* 2014; **52**:515–532.
20. Rashid MM, Selimotic M. A three-dimensional finite element method with arbitrary polyhedral elements. *International Journal for Numerical Methods in Engineering* 2006; **67**:226–252.
21. Duan Q, Li X, Zhang H, Belytschko T. Second-order accurate derivatives and integration schemes for meshfree methods. *International Journal for Numerical Methods in Engineering* 2012; **92**:399–424.
22. Brezzi F, Lipnikov K, Simoncini V. A family of mimetic finite difference methods on polygonal and polyhedral meshes. *Mathematical Models and Methods in Applied Sciences* 2005; **15**:1533–1551.

DOI: 10.1002/nme